Geophysical Research Letters

RESEARCH LETTER
10.1029/2020GL087529

Heterogeneity-Induced Mixing and Reaction Hot Spots Facilitate Karst Propagation in Coastal Aquifers

K. De Vriendt[1,2], **M. Pool**[1,3], **and M. Dentz**[1]

[1]Institute of Environmental Assessment and Water Research, IDAEA-CSIC, Barcelona, Spain, [2]Department of Civil and Environmental Engineering, Technical University of Catalonia (UPC), Barcelona, Spain, [3]AMPHOS 21 Consulting S. L., Barcelona, Spain

Key Points:
- Heterogeneity results in localized reactive hot spots across the entire mixing zone
- The presence of heterogeneity may provide an explanation for complex dissolution features observed in coastal karstic systems

Supporting Information:
- Supporting Information S1

Correspondence to:
M. Dentz,
marco.dentz@csic.es

Citation:
De Vriendt, K., Pool, M., & Dentz, M. (2020). Heterogeneity-induced mixing and reaction hot spots facilitate Karst propagation in coastal aquifers. *Geophysical Research Letters*, *47*, e2020GL087529. https://doi.org/10.1029/2020GL087529

Received 13 FEB 2020
Accepted 27 APR 2020
Accepted article online 29 APR 2020

Abstract The freshwater-seawater mixing zone is a critical region for chemical activity. Yet little is known about the influence of ever present spatial heterogeneity on the dynamics of mixing and calcite dissolution, which play a key role in the understanding of karst development. We analyze the impact of different heterogeneity structures and strengths on the local and global response of mixing and dissolution rates across the saltwater freshwater mixing zone. We find that the initial heterogeneity structure significantly impacts observed dissolution and mixing patterns, which sheds some new light on karst propagation in coastal aquifers.

1. Introduction

The mixing of freshwater and seawater in coastal carbonate formations has been long associated with zones of high porosity development and elaborate cave networks (Back et al., 1986). The presence of caves in the Yucatán Peninsula (Back et al., 1979, 1986; Stoessell & Schuffert, 1989) and enhanced porosity observed from cores collected in the Bermudas Andros island (Smart et al., 1988), for example, have been directly attributed to mixing dynamics across the salt-freshwater mixing zone. Despite this, limited accessibility to deeper portions of the mixing zone has prevented large-scale surveys of caves, which may otherwise be available further inland. Since the topology of many karstic networks and their subsequent geomorphological characteristics are strongly linked to their flow regimes and local geology (Jouves et al., 2017), understanding the behavior of mixing and reactions under variable density flow in coastal systems under the influence of various types of heterogeneity may offer insight into the localization of preferential calcite dissolution, which may be particularly important during the initial stages of karst propagation.

Numerical studies have previously demonstrated that calcite dissolution across the seawater-freshwater interface occurs dominantly across the fresher spectrum of the mixing zone where mixing waters are most strongly undersaturated with respect to calcite (Rezaei et al., 2005; Sanford & Konikow, 1989). Moreover, Sanford and Konikow (1989) found that dissolution takes place in fresher water then what would be expected by simple mixing alone. Interestingly, two reactive hot spots were also observed: one in fresher portion of the mixing zone at the toe and one in saltier portion of mixing waters at the discharge zone. These behaviors have been attributed to an initial-mixing effect at the toe, which gives way to the highest potential for undersaturation and enhanced dispersive mixing at the discharge zone. While these homogeneous studies have provided valuable insight into the interplay between transport and chemical reactions, they fall short of explaining the maze-like conduit networks observed in real karst aquifers.

Coastal carbonate aquifers present heterogeneous discontinuities, such as fractures, dikes, and large-scale stratification, which may induce complex salinity distributions leading to irregular patterns of enhanced local mixing and reactive hot spots, that is, zones of enhanced reactivity. It is well known that heterogeneity of hydraulic properties strongly controls solute spreading and mixing in porous media (Dagan, 1987; Dentz et al., 2011; Gelhar, 1993, 2003). Heterogeneity has also been suggested as an important mechanism toward realistic representations of mixing and offshore submarine groundwater discharge (Michael et al., 2016). However, only few studies have addressed heterogeneity for variable density flow systems and, in particular, for seawater intrusion problems (see, e.g., Abarca, 2006; Held et al., 2005; Kerrou & Renard, 2010; Kreyns et al., 2020; Pool et al., 2015; Sebben et al., 2015). In general, it has been shown that heterogeneity leads to increased spreading of the freshwater-seawater mixing zone. While it is evident that heterogeneity plays

a strong role in mixing in many subsurface groundwater problems, its impact on mixing-limited reactions such as calcite dissolution in coastal variable density flow systems remains an open question.

In this paper, we investigate the effect of heterogeneity and connectivity on mixing and chemical reactions across the salt-freshwater interface under steady-state conditions. We consider a fast calcite dissolution reaction to explore karstification processes induced by mixing in coastal aquifers. Two-dimensional (2-D) variable density flow and transport simulations are performed considering large-scale hydraulic conductivity stratification and log-normally distributed multi-Gaussian (MG) hydraulic conductivity fields. In addition, more complex heterogeneous fields characterized by connected and disconnected patterns of high and low conductivity are considered. We analyze the mixing and reaction dynamics by focusing on the local and global reaction and mixing rates. Our results aim to provide insight into the role of heterogeneity in nonuniform flow fields such as that induced by seawater intrusion.

2. Methods

We study mixing and calcite dissolution patterns under steady variable density flow in 2-D heterogeneous coastal aquifers. Density-dependent flow is described by the Darcy equation

$$\mathbf{q}(\mathbf{x}) = -K(\mathbf{x})\left[\nabla h_f(\mathbf{x}) + \frac{\rho(\mathbf{x}) - \rho_f}{\rho_f}\mathbf{e}_z\right], \tag{1}$$

where $\mathbf{x} = (x, z)^\top$ is the coordinate vector, $\mathbf{q}(\mathbf{x})$ the specific discharge, $K(\mathbf{x})$ hydraulic conductivity, $h_f(\mathbf{x})$ the equivalent freshwater head, $\rho(\mathbf{x})$ the fluid density, ρ_f the density of freshwater, and $\mathbf{e}_z$ the unit vector in z direction. Fluid mass conservation in the absence of sources and sinks implies $\nabla \cdot \rho(\mathbf{x})\mathbf{q}(\mathbf{x}) = 0$. The fluid density depends on the mixing ratio $c(\mathbf{x})$ between fresh and seawater and is assumed to be linearly dependent on the salt mass fraction $\omega(\mathbf{x})$ (mass of salt dissolved per unit mass of fluid) given by $\rho(\mathbf{x}) = \rho_f[1 + \beta c(\mathbf{x}, t)]$, where β is the buoyancy factor given by $\beta = (\rho_s - \rho_f)/\rho_f$ and ρ_s is the density of seawater. The mixing ratio is given by $c(\mathbf{x}) = \omega(\mathbf{x})/\omega_s$, with $\omega(\mathbf{x})$ the salt mass fraction in the mixture and ω_s the salt mass fraction of seawater. Thus, it obeys the steady-state advection-dispersion equation (Voss & Provost, 2002),

$$\mathbf{q}(\mathbf{x}) \cdot \nabla c(\mathbf{x}) - \nabla \cdot \left[\mathbf{D}(\mathbf{x}) + \phi D_m\right] \nabla c(\mathbf{x}) = 0, \tag{2}$$

with $\mathbf{D}(\mathbf{x})$ the dispersion tensor (Bear, 1988), D_m the molecular diffusion, and ϕ the porosity.

The flow domain is 1,500 m long and 100 m wide with a prescribed freshwater flux of 250 m/a and zero mixing ratio at the inland boundary at $x = 0$ and hydrostatic saltwater at the seaward boundary. The mixing ratio and the inland boundary are set to 0, while the mass flux at the seaward boundary is set equal to the advective flux of seawater if the horizontal component of $\mathbf{q}$ point inland and equal to the advective flux of the local mixing ratio otherwise. We choose a ratio of $1/2$ between transverse and longitudinal dispersivities (Abarca & Clement, 2009; Robinson et al., 2015). A detailed relation of the numerical setup and parameters can be found in section 3 of the supporting information. Hydraulic conductivity $K(\mathbf{x})$ is modeled as a 2-D spatial random field. We consider MG, as well fields of connected high (C_f) and low hydraulic conductivity (D_f). All fields are characterized by log-normal point statistics with variances of the log hydraulic conductivity $\sigma^2_{lnK} = 1$ and 3. The connected high (C_f) and low hydraulic conductivity (D_f) serve to mimic the presence of channels or fractures.

In order to highlight the influence of heterogeneity on mixing and reaction efficiency, we compare the results from the heterogeneous to equivalent homogeneous scenarios. For each type of heterogeneity and log-K variance, 10 equally probable realizations are considered. The observables presented in the following are obtained by averaging over the set of realizations for each heterogeneity type (averaged quantities are denoted by an overline). While we consider only a limited number of realizations due to computational constraints, the variability between realizations is low such that the average can be considered representative for the heterogeneity impact on the mixing and reaction behavior. Furthermore, in order to illustrate reactive patterns that may emerge in the presence of large-scale discontinuities, we consider in section 3.3 two realizations of a stratified MG aquifer structure characterized by infinite longitudinal correlation length, transverse correlation length of 10 m, and $\sigma^2_{lnK} = 1$ and 3. Details on the model setup and parameters are given in section 4 of the supporting information.

Figure 1a illustrates maps of the mixing ratio and velocity magnitude for homogeneous, MG, connected, and disconnected hydraulic conductivity fields. The mixing area $\overline{A}_m$ between fresh and seawater shown in

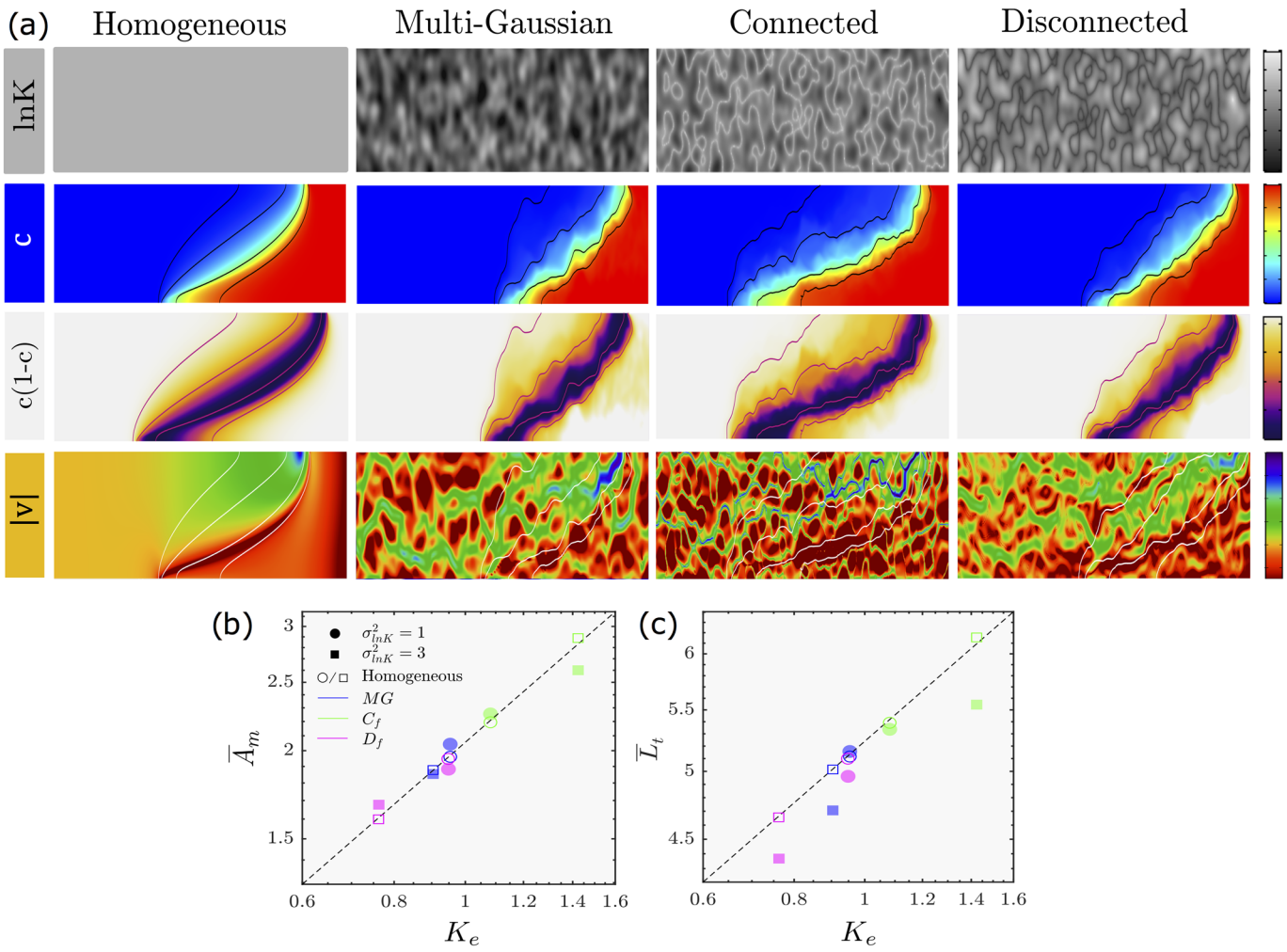

Figure 1. Maps showing examples of (from top to bottom) the hydraulic conductivity field for the homogeneous and heterogeneous fields ($\sigma^2_{lnK} = 1$), the mixing ratio (c), $c(1-c)$, and the logarithm of the velocity modulus ($|v|$). (b) The nondimensional average mixing area ($\overline{A}_m$) and (c) the toe position ($\overline{L}_t$) against their nondimensional hydraulic conductivity (K_e). The dashed lines denote the dependence of the mixing area and toe position on hydraulic conductivity for an equivalent homogeneous medium. Mixing ratio contours displayed in the maps correspond to mixing ratios of 1%, 10%, 50%, and 95%.

Figure 1b is defined as the area comprised between the 0.95 and 0.01 isolines of the mixing ratio. The penetration depth $\overline{L}_t$ of the seawater wedge shown in Figure 1c is defined as the distance of the 0.5 isoline of the mixing ratio from the seaside boundary. Note that both these quantities are averaged across all realizations. The mixing area and penetration depth are nondimensionalized in terms of the characteristic length scale l_c, which here is identified with the height of the domain.

In order to investigate the influence of heterogeneity on mixing and reaction efficiency, we compare the results from the heterogeneous realizations to equivalent homogeneous media. In order to determine the effective hydraulic conductivity of the equivalent media, a constant hydraulic head gradient is imposed between the inland and the seaside boundaries for each heterogeneous realization, with the horizontal boundaries defined as no-flow boundaries. The effective hydraulic conductivity K_e is given by the ratio between the total flow rate across the seaside boundary and the average hydraulic head gradient. The effective hydraulic conductivity is nondimensionalized by the geometric mean conductivity K_g, which for all fields under consideration is $K_g = 5 \cdot 10^{-4}$ m/s. Note that for isotropic MG fields, K_g is equal to the effective conductivity (see, e.g., Renard & de Marsily, 1997; Sanchez-Vila et al., 2006). As evidenced in Figures 1b and 1c, $\overline{K}_e$ corresponds well to the level of connectivity of each field. As found by Zinn and Harvey (2003), connectivity results in an increase in $\overline{K}_e$. Furthermore, as observed for MG heterogeneous media (Abarca, 2006; Kerrou & Renard, 2010), we see in Figures 1b and 1c that both $\overline{L}_t$ and $\overline{A}_m$ decrease with increasing

heterogeneity. This can be directly linked to a decrease in $\overline{K}_e$. For the connected fields, $\overline{K}_e$ increases with increasing heterogeneity. In general, we see that increase or decrease in $\overline{K}_e$ directly corresponds to increase or decrease in toe length and mixing area for both the homogeneous and heterogeneous fields.

The mixing and reaction behavior and its impact on karst propagation are studied through the process of mixing-induced calcite dissolution. In the considered setting, we use the two representative end-members of freshwater and seawater according to Rezaei et al. (2005). The seawater composition represents water collected from boreholes in a coastal aquifer from Grand Cayman (Ng & Jones, 1995), while the freshwater composition represents distilled water in equilibrium with calcite; see Table S1 for the details of the chemical system. When the respective equilibria are perturbed due to mixing, the new chemical equilibrium of the mixture is established instantaneously. This is a reasonable assumption for coastal aquifers where calcite dissolution is fast relative to the residence times of water (Rezaei et al., 2005; Sanford & Konikow, 1989). We consider the chemical system detailed in De Simoni et al. (2007) under conditions that lead to undersaturation upon mixing and thus calcite dissolution. Note that this study does not incorporate any feedback between chemical reactions and the flow and transport properties. The equilibrium reaction rate can then be written in the form

$$r(\mathbf{x}) = \Lambda(\mathbf{x})\chi(\mathbf{x}), \tag{3}$$

where $\chi(\mathbf{x})$ is the local mixing rate,

$$\chi(\mathbf{x}) = \nabla c(\mathbf{x}) \cdot \left[\mathbf{D}(\mathbf{x}) + \phi D_m\right] \nabla c(\mathbf{x}). \tag{4}$$

Reaction and mixing rates are nondimensionalized in the following according to $r' = r l_c / q_f \sqrt{K_{eq}}$, and $\chi' = \chi l_c^2 / \alpha_g q_f$, where α_g is the geometric mean of the longitudinal and transverse dispersivities, q_f is the inland freshwater flux, and K_{eq} is the solubility product for calcite dissolution. In the following, we omit the primes for simplicity of notation. The mixing rate χ measures the dynamics of conservative mixing between fresh and saltwater. The chemistry is contained in the speciation intensity Λ as outlined in detail in section 2 of the supporting information. Note that the term equilibrium reaction rate may appear contradictory; however, it describes the rate of reaction due to fast chemical equilibration of two end-members upon mixing. Therefore, it is dominated by the mixing rate χ, whose magnitude depends on both concentration gradients and dispersion coefficients. In our analysis, we assess the average scalar dissipation rate $\langle\chi\rangle$ and reaction rate $\langle r\rangle$ per unit mixing area. This facilitates the intercomparison of heterogeneous fields with respect to the corresponding homogeneous scenarios.

3. Results and Discussion

We discuss here the impact of heterogeneity on mixing and dissolution patterns and their subsequent implications on the propagation of karsts.

3.1. Influence of Heterogeneity on Mixing Rate

Figure 2 shows the strong impact that the presence of heterogeneity has on both the mixing and reaction rate across the interface. At the top of the transition zone, high velocities induced by the freshwater discharge translate to strong dispersive mixing (Rezaei et al., 2005). This is reflected in χ for both the homogeneous and heterogeneous media. It can be observed that heterogeneity-induced velocity variations lead to both greater variability and the steepening of concentration gradients resulting in enhanced mixing along the mixing interface. As expected, since χ depends on both the presence of concentration gradients and dispersion, the largest values are localized in high-K zones, where velocities and thus dispersion are large. Note that while χ is generally highest along the 50% mixing ratio contour, near the toe, it extends into the fresher portion of the mixing zone. This can be attributed to enhanced interface compression that accompanies a stagnation point (see, e.g., Hidalgo & Dentz, 2018; Ranz, 1979), which, for the seawater intrusion problem, exists at the toe. This observation suggests that the localized hot spot at the toe is not simply the result of the previously mentioned initial-mixing effect (Rezaei et al., 2005; Sanford & Konikow, 1989) but also due to strong flow deformation.

As shown in Figure 2c, $\langle\chi\rangle$ decreases linearly with increasing effective hydraulic conductivity for homogeneous media. There are two factors dominating $\langle\chi\rangle$. We first observe that the presence of hetereogeneity in general and the value of log-K variance in particular result in an increase of $\langle\chi\rangle$ for all fields with respect to

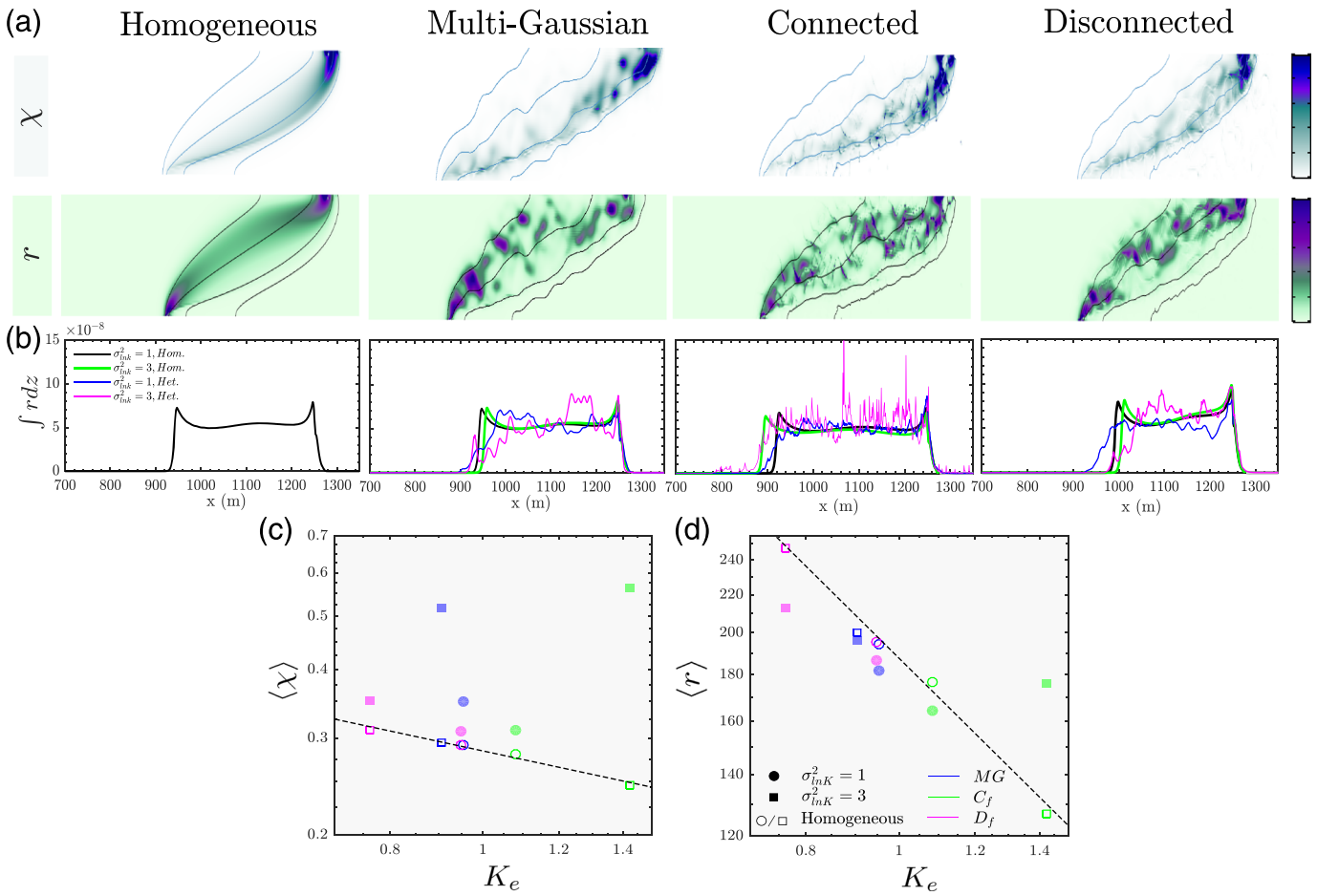

Figure 2. Examples of maps for ($\sigma^2_{lnK} = 3$) corresponding to (from top to bottom) the average mixing and reaction rates and the vertically integrated reaction rate for the homogeneous, multi-Gaussian (MG), connected (C_f), and disconnected fields (D_f). The scatter plot at the bottom shows the average nondimensional mixing rate ($\langle \chi \rangle$) and nondimensional reaction rates ($\langle r \rangle$) for their corresponding nondimensional effective hydraulic conductivities $\overline{K}_e$. Mixing ratio contours displayed in the maps correspond to mixing ratios of 1%, 10%, 50%, and 95%. The dashed lines denote the dependence of the mixing and reaction rate on hydraulic conductivity for an equivalent homogeneous medium.

their homogeneous equivalent. This is most notable for the connected scenarios, for which the mixing rate increases up to a factor of 2. Additionally, we see that K_e strongly controls the behavior of $\langle \chi \rangle$ for homogeneous and weakly heterogeneous fields. This may be understood as follows. For high K_e, the interface penetrates further and is flatter than for low K_e. Thus, at high K_e, there is a lower velocity contrasts between the flowing freshwater body and the convection cell at the seaside boundary. Reduction of velocity contrast leads to a reduction of concentration contrast, which in turn reduces the mixing rate.

3.2. Influence of Heterogeneity on the Reaction rate

In accordance with the studies of Sanford and Konikow (1989) and Rezaei et al. (2005), zones of enhanced calcite dissolution are shown to occur near the fresher spectrum of the mixing zone (see Figure 2a). This is once again due to the fact that the speciation intensity, which is a nonlinear function of the mixing ratio, concentrates at the freshwater dominated part of the mixing zone. In fact, reaction hot spots may be due to a high local speciation intensity in a moderate mixing background, or due to a high mixing rate in a background of moderate speciation intensity. For the homogeneous scenarios, as expected, one observes two significant reaction hot spots at the top and bottom of the mixing zone. The reaction hot spot at the top of the aquifer coincides with the mixing hot spot, while the reaction hot spot at the toe is determined by high speciation intensity in the presence of moderate mixing. Our simulations reveal that heterogeneity induces highly irregular distributions of reaction rates that strongly deviate from the homogeneous case.

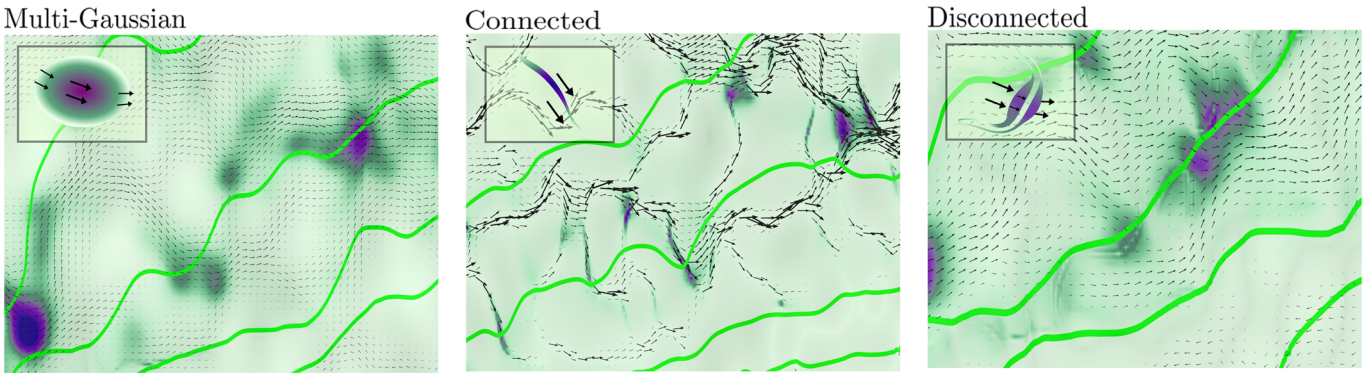

Figure 3. Zoomed-in sections of the reaction field overlaid with their corresponding hydraulic conductivity field. Arrows represent flow directions whose length is proportional to the logarithm of velocity.

This is further evidenced in Figure 2b, which shows the vertically integrated heterogeneous reaction rate profiles compared to their respective effective homogeneous behavior. In the presence of heterogeneity, distinct reaction hot spots emerge along the interface whose density and intensity increase with increasing heterogeneity and also with the connectivity. Thus, spatial heterogeneity broadens the spectrum of local reaction rates toward high values compared to homogeneous media. In Figure 2d, we observe that, for the exception of the high variance connected field, $\langle r \rangle$ is smaller for heterogeneous fields compared to the respective homogeneous case. This can be understood by the increased segregation of high-K zones, where reactions preferentially occur. In the case of the high variance connected field, an increase in $\langle r \rangle$ compared to the homogeneous scenario can be attributed to the strongly enhanced mixing rates observed in Figure 2c, which permits reactions to occur over a larger portion of the mixing zone.

While the spatial variability of reactions is strongly impacted by the presence of heterogeneity, we see that, similar to the behavior of $\langle \chi \rangle$ for homogeneous and weakly heterogeneous scenarios, $\overline{K}_e$ exerts a strong control over $\langle r \rangle$, even for the higher log-K variance disconnected and MG fields. It should be reiterated that while an increase in $\overline{K}_e$ lengthens the interface, which increases the area over which mass transfer can occur, the velocity and concentration contrasts at the mixing interface are higher when the toe is closer to the seaside boundary, resulting in higher averaged reaction rates per unit area.

3.3. Influence of Heterogeneity on Reactive Patterns

The type of imposed heterogeneity manifests in particular patterns of enhanced reactivity in the presence of the nonuniform flow field. MG fields, for example, are characterized by hot spots that radiate concentrically, while connected field hot spots are predominantly isolated in high-K channels that are orientated vertically, parallel to the local direction of flow. For the disconnected field, reaction patterns are qualitatively similar to MG fields, but they also contain zones of enhanced reaction that straddle low-K channels, perpendicular to the local direction of flow, as can be seen in Figure 3. It is interesting to note that despite the apparent connectivity of the imposed heterogeneous structures, zones of enhanced reactivity tend to emerge as unconnected features. This suggests that during early stages of diagenesis, the spatial location and orientation of hydraulic features during seawater intrusion may strongly control the transient evolution of caves. It is possible however that in the presence of temporal fluctuations, the movement of the wedge back and forth over large timescales may be the precursor to connecting these localized reactive hot spots into the maze-like features we observe today.

Note that the connected and disconnected conductivity fields under consideration so far shed some light onto possible dissolution patterns and pattern formation during calcite dissolution. However, they are highly nonlinear and tortuous and do not reproduce structures similar to networks of linear fractures typical for fractured carbonates. A different approach, similar to discrete fracture networks, is needed in order to assess this type of situations. However, in order to get some insight into calcite dissolution in the presence of large-scale connectivity, we consider horizontally stratified conductivity fields. We observe that vertical changes in hydraulic conductivity cause strong velocity and concentration contrast across the mixing interface, which manifests as narrow, elongated zones of enhanced reactivity. In Figure 4, we see that by increasing the log-K variance, the strong concentration gradient along the low-K layers leads to

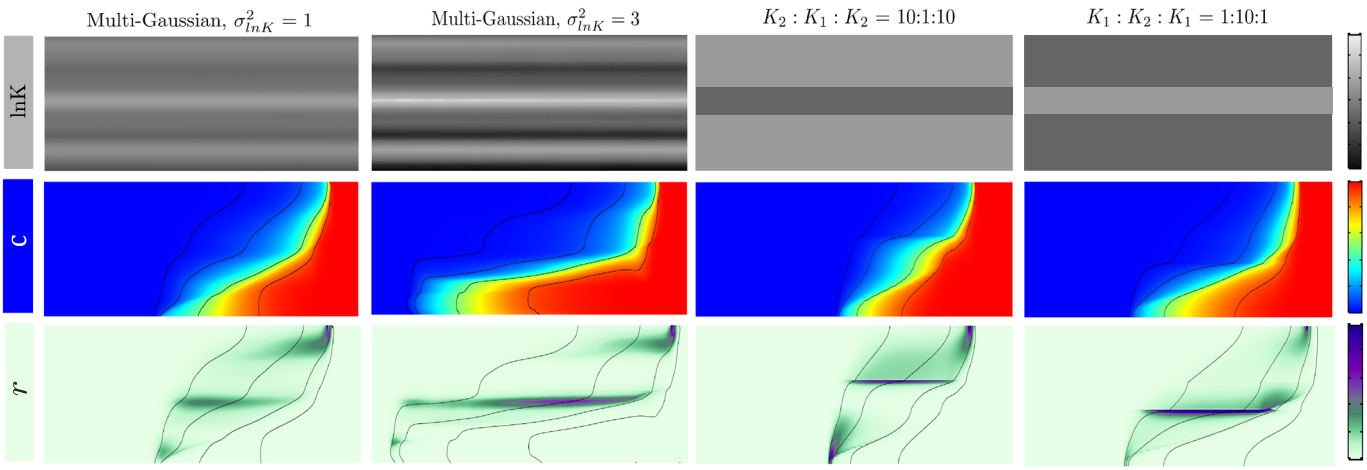

Figure 4. Horizontally stratified hydraulic conductivity fields. From top to bottom are the log K, the mixing ratio, and reaction rate fields. The two leftmost columns show the results for the multi-Gaussian stratified scenario for $\sigma^2_{lnK} = 1$ and 3, while the two rightmost columns show the results for an aquifer whose hydraulic conductivity is discretely layered. The third column shows the results for a K ratio of 10:1:10, while the fourth column shows the result for a K ratio of 1:10:1.

enhanced reactions. In addition to the stratified MG fields, simulations for discrete low-high-low (1:10:1) and high-low-high (10:1:10) further isolate these dynamics. We see that when a low-conductive material sandwiches a high-conductive layer, strong dissolution occurs at the base of the high-K zone, whereas strongest dissolution is observed at the top of the stratified layer for the high-low-high K scenario. This illustrates that reaction is enhanced when flow is directed from a low- to high-K medium, which sheds light on the preferential development of karstic systems.

Another important point to note is that karstification is inherently a 3-D process. While our study is 2-D, the fundamental mechanisms relating medium structure, flow heterogeneity, and mixing and dissolution are expected to be qualitatively similar in 3-D. We expect that 3-D connectivity fields are more connected than 2-D fields, which may quantitatively alter the flow deformation, mixing, and thus the dissolution rates. Due to the additional spatial dimension and 3-D structure, one could expect a stronger deformation action of the underlying flow field and thus higher mixing rates (Cirpka et al., 2015; Chiogna et al., 2015; Ye et al., 2015a, 2015b). However, these features do not affect the basic mechanisms that lead to the localization of dissolution hot spots based on the initial medium and flow structure.

4. Concluding Remarks

The topology of karst conduits has been strongly linked to their spatial location and the governing flow characteristics (e.g., Audra & Palmer, 2015; Gabrov et al., 2014; Palmer, 1992). For example, anastomosic caves, defined by their braided patterns, typically occur across bedding planes in the epiphreatic zone, whereas angular mazes tend to be associated with fractured media due to seepage from overlying insoluble rocks (Jouves et al., 2017). While near-surface features such as flank margin caves (Mylroie et al., 1990) can be observed in many coastal carbonate environments along the salt-freshwater mixing zone, limited accessibility has prevented large-scale speleological surveys of karst conduits in coastal aquifer. Consequently, no formal characteristics exist to describe dissolution patterns at depth across the mixing zone. It is therefore possible that many hydraulically dominant karstic features may exist outside our current ability to observe.

Our study suggests that the initial stages of karst development, also known as the laminar flow phase (Lowe, 1992), may be a crucial period, which influences the subsequent evolution of a karstic conduit. The importance of early-stage karst development was also investigated by Groves and Howard (1994), who found that enlargement of conduits in coastal carbonate aquifers occurs very selectively during the laminar flow regime. Geomorphological studies on phreatic karstic caves have shown that over 70% of conduits develop along discrete bedding planes in limestones (Filipponi et al., 2009), known as “inception horizons” (Lowe, 1992). Such features are the result of physical, lithological, and chemical deviations from the central carbonate facies. Cave surveys have shown that inception horizons may play a strong role during the most early stages of karst formation (Filipponi et al., 2009). In the simplest case of large-scale horizontal

stratification, our study suggests that in coastal environments, due to the density-driven convection and subsequent upward recirculation of flow, even simple changes in hydraulic conductivity could be very sensitive to enhanced dissolution. Sanford and Konikow (1989) showed that a migrating seawater wedge in a homogeneous media results in increased permeability, which would consequently shift the wedge further inland. One could therefore imagine that large-scale sea level and tidal fluctuations generate elongate karstic features that extend many kilometers inland.

Acknowledgments
Data associated with this manuscript are available in the DIGITAL.CSIC repository at https://digital.csic.es/ under the DOI (https://doi.org/10.20350/digitalCSIC/8955). This project has received funding from the European Union's Horizon 2020 research and innovation program under the Marie Skłodowska Curie Grant Agreement No. 722028 (ENIGMA ITN). Maria Pool acknowledges the support of the Spanish Ministry of Science and Innovation through the Torres-Quevedo program.

References

Abarca, E. (2006). Seawater intrusion through heterogeneous aquifers (Ph.D. thesis), Universitat Politécnica de Catalunya.

Abarca, E., & Clement, T. P. (2009). A novel approach for characterizing the mixing zone of a saltwater wedge. *Geophysical Research Letters*, *36*, L06402. https://doi.org/10.1029/2008GL036995

Audra, P., & Palmer, A. (2015). Research frontiers in speleogenesis. Dominant processes, hydrogeological conditions and resulting cave patterns. *Acta Carsologica*, *44*(3), 315–348. https://doi.org/10.3986/ac.v44i3.1960

Back, W., Hanshaw, B. B., Pyle, T. E., Plummer, L. N., & Weidie, A. E. (1979). Geochemical significance of groundwater discharge and carbonate solution to the formation of Caleta Xel Ha, Quintana Roo, Mexico. *Water Resources Research*, *15*(6), 1521–1535. https://doi.org/10.1029/WR015i006p01521

Back, W., Hanshaw, B. B., Survey, U. S. G., Herman, J. S., Sciences, E., Driel, J. N. V., & Survey, U. S. G. (1986). Differential dissolution of a Pleistocene reef in the ground-water mixing zone of coastal Yucatan, Mexico. *Geology*, *14*(February), 137–140.

Bear, J. (1988). *Dynamics of fluids in porous media*. inc New York: Dover publications.

Chiogna, G., Cirpka, O. A., Rolle, M., & Bellin, A. (2015). Helical flow in three-dimensional nonstationary anisotropic heterogeneous porous media. *Water Resources Research*, *51*, 261–280. https://doi.org/10.1002/2014wr015330

Cirpka, O. A., Chiogna, G., Rolle, M., & Bellin, A. (2015). Transverse mixing in three-dimensional nonstationary anisotropic heterogeneous porous media. *Water Resources Research*, *51*, 241–260. https://doi.org/10.1002/2014wr015331

Dagan, G. (1987). Theory of solute transport by groundwater. *Annual Review of Fluid Mechanics*, *19*(1), 183–213. https://doi.org/10.1146/annurev.fluid.19.1.183

De Simoni, M., Carrera, J., & Saaltink, M. W. (2007). A mixing ratios-based formulation for multicomponent reactive transport. *Water Resources Research*, *43*, W07419. https://doi.org/10.1029/2006WR005256

De Vriendt, K., Pool, M., & Dentz, M. (2020). Supporting Information for "Heterogeneity-induced mixing and reaction hotspots facilitate Karst propagation in coastal aquifers".

Dentz, M., Le, T., Englert, A., & Bijeljic, B. (2011). Mixing, spreading and reaction in heterogeneous media: A brief review. *Journal of Contaminant Hydrology*, *120-121*, 1–17. https://doi.org/10.1016/j.jconhyd.2010.05.002

Filipponi, M., Jeannin, P.-Y., & Tacher, L. (2009). Geomorphology evidence of inception horizons in karst conduit networks. *Geomorphology*, *106*(1-2), 86–99. https://doi.org/10.1016/j.geomorph.2008.09.010

Gabrov, F., Häuselmann, P., & Audra, P. (2014). 'Looping caves' versus 'water table caves': The role of base-level changes and recharge variations in cave development. *Geomorphology*, *204*, 683–691. https://doi.org/10.1016/j.geomorph.2013.09.016

Gelhar, L. W. (1993). *Stochastic subsurface hydrology*. Englewood Cliffs, NJ: Prentice-Hall.

Gelhar, L. W. (2003). *Applied stochastic hydrogeology*. New York, NY: Oxford University Press.

Groves, C. G., & Howard, A. (1994). Early development of karst systems. I. Preferential flow path enlargement under laminar flow. *Water Resources Research*, *30*(10), 2837–2846. https://doi.org/10.1029/94WR01303

Held, R., Attinger, S., & Kinzelbach, W. (2005). Homogenization and effective parameters for the Henry problem in heterogeneous formations. *Water Resources Research*, *41*, W11420. https://doi.org/10.1029/2004WR003674

Hidalgo, J. J., & Dentz, M. (2018). Mixing across fluid interfaces compressed by convective flow in porous media. *Journal of Fluid Mechanics*, *838*, 105–128. https://doi.org/10.1017/jfm.2017.888

Jouves, J., Jouves, J., Viseur, S., Ar, B., Baudement, C., & Camus, H. (2017). Speleogenesis, geometry, and topology of caves: A quantitative study of 3D karst conduits. *Geomorphology*, *298*, 86–106. https://doi.org/10.1016/j.geomorph.2017.09.019

Kerrou, J., & Renard, P. (2010). A numerical analysis of dimensionality and heterogeneity effects on advective dispersive seawater intrusion processes. *Hydrogeology Journal*, *18*(1), 55–72. https://doi.org/10.1007/s10040-009-0533-0

Kreyns, P., Geng, X., & Michael, H. A. (2020). The influence of connected heterogeneity on groundwater flow and salinity distributions in coastal volcanic aquifers. *Journal of Hydrology*, *586*, 124,863. https://doi.org/10.1016/j.jhydrol.2020.124863

Lowe, D. J. (1992). The origin of limestone caverns: An inception horizon hypothesis (Ph.D. thesis), Manchester Polytechnic.

Michael, H. A., Scott, K. C., Koneshloo, M., Yu, X., Khan, M. R., & Li, K. (2016). Geologic influence on groundwater salinity drives large seawater circulation through the continental shelf. *Geophysical Research Letters*, *43*, 10,782–10,791. https://doi.org/10.1002/2016GL070863.Received

Mylroie, J. E., Carew, J. L., Mylroie, J. E., & Carew, J. L. (1990). The flank margin model for dissolution cave development in carbonate platforms. *Earth Surface Processes and Landforms*, *15*(5), 413–424. https://doi.org/10.1002/esp.3290150505

Ng, K. C., & Jones, B. (1995). Hydrogeochemistry of Grand Cayman, British West Indies: Implications for carbonate diagenetic studies. *Journal of Hydrology*, *164*(1-4), 193–216. https://doi.org/10.1016/0022-1694(94)02556-Q

Palmer, A. (1992). Origin and morphology of limestone caves. *Geological Society of America Bulletin*, *103*(1), 1–21.

Pool, M., Post, V. E. A., & Simmons, C. T. (2015). Effects of tidal fluctuations and spatial heterogeneity on mixing and spreading in spatially heterogeneous coastal aquifers. *Water Resources Research*, *51*, 1570–1585. https://doi.org/10.1002/2014WR016068

Ranz, W. E. (1979). Applications of a stretch model to mixing, diffusion, and reaction in laminar and turbulent flows. *The American Institute of Chemical Engineers*, *25*(1), 41–47.

Renard, P., & de Marsily, G. (1997). Calculating equivalent permeability: A review. *Advances in Water Resources*, *20*(5-6), 253–278.

Rezaei, M., Sanz, E., Raeisi, E., & Ayora, C. (2005). Reactive transport modeling of calcite dissolution in the fresh-salt water mixing zone. *Journal of Hydrology*, *311*, 282–298. https://doi.org/10.1016/j.jhydrol.2004.12.017

Robinson, G., Hamill, G. A., & Ahmed, A. A. (2015). Automated image analysis for experimental investigations of salt water intrusion in coastal aquifers. *Journal of Hydrology*, *530*, 350–360. https://doi.org/10.1016/j.jhydrol.2015.09.046

Sanchez-Vila, X., Guadagnini, A., & Carrera, J. (2006). Representative hydraulic conductivities in saturated groundwater flow. *Reviews of Geophysics*, *44*, RG3002.

Sanford, W. E., & Konikow, L. F. (1989). Simulation of calcite dissolution and porosity changes in saltwater mixing zones in coastal aquifers. *Water Resources Research*, *25*(4), 655–667.

Sebben, M. L., Werner, A. D., & Graf, T. (2015). Seawater intrusion in fractured coastal aquifers: A preliminary numerical investigation using a fractured Henry problem. *Advances in Water Resources*, *85*, 93–108. https://doi.org/10.1016/j.advwatres.2015.09.013

Smart, P. L., Dawans, J. M., & Whitaker, F. (1988). Carbonate dissolution in a modern mixing zone. *Nature*, *335*(6193), 811–813. https://doi.org/10.1038/335811a0

Stoessell, R. K., & Schuffert, J. D. (1989). Water chemistry and $CaCO_3$ dissolution in the saline part of an open flow mixing zone, coastal Yucatan Peninsula, Mexico. *Geological Society of America Bulletin*, *101*, 159–169.

Voss, C. I., & Provost, A. (2002). A model for saturated-unsaturated variable-density ground-water flow with solute or energy transport (*Tech. rep*).

Ye, Y., Chiogna, G., Cirpka, O., Grathwohl, P., & Rolle, M. (2015a). Experimental evidence of helical flow in porous media. *Physical Review Letters*, *115*(19). https://doi.org/10.1103/physrevlett.115.194502

Ye, Y., Chiogna, G., Cirpka, O., Grathwohl, P., & Rolle, M. (2015b). Experimental investigation of compound-specific dilution of solute plumes in saturated porous media: 2-D vs. 3-D flow-through systems. *Journal of Contaminant Hydrology*, *172*, 33–47. https://doi.org/10.1016/j.jconhyd.2014.11.002

Zinn, B., & Harvey, C. F. (2003). When good statistical models of aquifer heterogeneity go bad: A comparison of flow, dispersion, and mass transfer in connected and multivariate Gaussian hydraulic conductivity fields. *Water Resources Research*, *39*(3), 1–19. https://doi.org/10.1029/2001WR001146